The Interpretation of Sulfur K-Edge XANES Spectra: A Case Study on Thiophenic and Aliphatic Sulfur Compounds

A. Mijovilovich,[†] L. G. M. Pettersson,[‡] S. Mangold,[§] M. Janousch,[||] J. Susini,[⊥] M. Salome,[⊥] F. M. F. de Groot,[†] and B. M. Weckhuysen*,[†]

Inorganic Chemistry and Catalysis group, Debye Institute for Nanomaterials Research, Department of Chemistry, Utrecht University, Sorbonnelaan 16, 3584CA, Utrecht, The Netherlands, Department of Physics, AlbaNova, Stockholm University, SE 106 9 L Stockholm, Sweden, ANKA, Forschungszentrum Karlsruhe GmbH, Institut für Synchrotronstrahlung (ISS), Hermann-von-Helmholtz-Platz 1, D-76344 Eggenstein, Germany, Swiss Light Source, Paul Scherrer Institute, CH 5232 Villigen, Switzerland, and X-ray Microscopy beamline, ID21, European Synchrotron Radiation Facility, 6 rue Jules Horowitz, BP 220, F-38043 Grenoble Cedex, France

Received: July 31, 2008; Revised Manuscript Received: December 20, 2008

Sulfur K-edge XANES has been measured for three sulfur model compounds, dibenzothiophene, dibenzothiophene sulfone, and aliphatic sulfur (DL-methionine). The spectra have been simulated with Density Functional Theory (DFT) by using a number of methods, including the half-core-hole approximation. Dipole transition elements were calculated and the transitions were convoluted with linearly increasing Gaussian functions in the first 20 eV of the near-edge region. In the case of dibenzothiophene, relaxation of the first excited states in the presence of the core-hole gave a further improvement. The theoretical results reproduce well the features of the spectra and give insight in the relation between geometric structure and molecular orbitals. Though DL-methionine and dibenzothiophene show a similar sharp rise of the white line, their molecular levels are quite different, pointing out the difficulties in finding useful "fingerprints" in the spectra for specific compounds.

Introduction

The activity of many proteins and enzymes is strongly modified if the thiol groups in the sulfur-containing amino acids cysteine and methionine are oxidized. In the case of oxidative stress, knowledge of the reversible process of oxidation−reduction of the thiols thus becomes of importance. Formation of disulfide bonds in proteins may furthermore drastically alter their function and here sulfur K-edge XANES (X-ray absorption near-edge structure) has been used to determine the thiol/disulfide ratio.[1] Spectrum deconvolution to determine what sulfur species are present has also been achieved in living tissue.[2,3] In archeology, knowledge of the different forms of sulfur is important for the understanding of the preservation of ancient artifacts when taken from "anaerobic" to "aerobic" environments.[4,5] Knowledge of the forms of sulfur and quantifying their occurrence is important in soil studies[6,7] and in crude oil production for improving desulfurization processes to give transportation fuels with low sulfur content.[8−10]

Crude oils are becoming increasingly heavier and with higher sulfur content. During the refinement, the hydrogenation and desulfurization have to be increased to maintain acceptable levels of product quality. Moreover in an increasingly environmentally aware society, sulfur is an undesired component in transportation fuels. The most difficult compounds for "deep desulfurization" are the higher molecular weight dibenzothiophenes with sterically hindered sulfur sites.[11] Different catalysts are employed with different specificity for sulfur compounds and different performance for the various desulfurization reactions, making it essential to know the composition of crude oils at the molecular level. Proper definition and speciation of the compounds will allow identifying the refinement steps that need to be improved.

XANES has been claimed to be insensitive to structural differences for compounds sharing the same sulfur functional group.[12] In reduced forms of sulfur (elemental sulfur, pyrite, sulfides, and thiophenes), the 1s to 3p transitions are close in energy, leading to about 10% uncertainty in determining the sulfur compounds through spectrum deconvolution.[9−11] However, the large chemical shift of about 14 eV for a valence range from −2 to 6, and the variety of near-edge structures, makes the technique suitable for component analysis in oils. In such analyses, the position and intensity of the first resonance in the K-edge ("white line") is used for speciation and quantification of the sulfur compounds. Nevertheless, modifications of the orbitals (due to medium, pH, protonation, etc.) from those of the model compounds can result in modifications of both K-edge positions and intensities, which may alter the determination of speciation. Thus, it is important to be able to assess a priori those modifications in determining a proper set of standard compounds representative of different chemical groups. Simulations of the sulfur K edge X-ray absorption spectroscopy (XAS) spectra can relate these effects to the modifications of the molecular orbitals. Density functional theory (DFT) calculations of the so-called "ligand K-edge XAS" provide information on the covalency of the S ligand to a metal, which has been recently exploited in bioinorganic and inorganic chemistry.[13] The obtained ground state density of states (DOS) on the sulfur seems reduced by 10−20% with respect to that of the core-excited final state.[14]

---

* To whom correspondence should be addressed. E-mail: b.m.weckhuysen@uu.nl.
[†] Utrecht University.
[‡] Stockholm University.
[§] Institut für Synchrotronstrahlung (ISS).
[||] Paul Scherrer Institute.
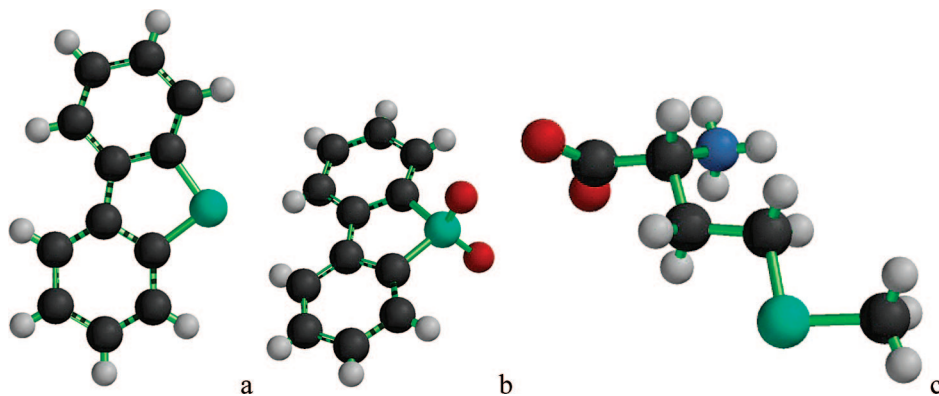[⊥] European Synchrotron Radiation Facility.

Figure 1. Structures of dibenzothiophene [DBZTHP01.CIF], dibenzothiophene sulfone [DBTHPS.cif], and DL-Methionine [DLMETA05.cif].

The intensity, $I(\omega)$, at frequency ω of an X-ray absorption spectrum is described with the Fermi golden rule, which with the single-electron excitation model in the dipole approximation can be written as (atomic units used):

$$I(\omega) \approx \frac{1}{\omega} \sum_f |\langle i|\hat{\mathbf{p}}|f\rangle|^2 \delta(E_i + \omega - E_f) =$$

$$\sum_f |\langle i|\hat{\mathbf{r}}|f\rangle|^2 \omega \delta(E_i + \omega - E_f) \quad (1)$$

The summation is over all final states $|f\rangle$ and the expressions for both the velocity and length forms are given. In cases where the transition moment $|\langle i|\hat{\mathbf{p}}|f\rangle|^2$ varies slowly with excitation energy the intensity $I(\omega)$ may be approximated[15] as a matrix element (M) times the density, $\rho(\omega)$, of empty states at energy ω, i.e., $I(\omega) \approx M^2\rho(\omega)$.

$\rho(\omega)$ must be calculated in the final state, that is in the presence of the core-hole. In periodic band structure calculations the requirement that the periodically repeated core-holes do not interact demands the use of a large supercell, which can make the calculations very time consuming. Such calculations have been performed for SiO_2,[16] $TiSi_2$,[17,18] and $LiCoO_2$,[19,20] as well as using a parametrized core-hole for Cu_2O.[21] In all cases the (full) core-hole calculation was much closer to experiment than the ground state calculation. Although, in general, the influence of the core-hole cannot be neglected, ground state calculations can still be relevant to approximate XAS. In some cases of oxygen K-edge spectra of metal-oxide solids, the ground state DOS seems to simulate the spectral shapes well.[22,23] For liquid and solid water, on the other hand, the specific treatment of the core-hole and related energy corrections for molecules in a different environment have been shown to have large effects on the spectral shape.[24–26] To investigate the performance of the ground state DOS approximation in the case of sulfur we suggest here to compare the sulfur K-edge spectra to the computed final and ground state DOS. Simulations of XANES spectra using DFT with the StoBe-deMon code[27] have proven to successfully model the sulfur K-edges in the case of sulfites, and also in methionine, methionine sulfoxide, cysteine, and cystine.[28,29] In these compounds the effects of solvation, protonation, and pH have been reproduced in the simulations. The results show the influence of pH and hydrogen bonding on the molecular orbitals.

Here, we simulate the sulfur K-edge XANES for three model compounds containing thiophenic (dibenzothiophene and dibenzothiophene sulfone) and aliphatic (DL-methionine) sulfur. While thiophenes constitute the most abundant fraction of sulfur

compounds in crude oil after desulfurization, methionines are very important in enzymatic redox processes. Thus, these compounds provide a good starting point to understand the influence on the spectrum profile of the molecular orbitals of these selected functional groups.

Materials and Methods

Dibenzothiophene, dibenzothiophene sulfone, and DL-methionine, further denoted as DBT, DBTS, and DLM, respectively, were purchased from Sigma Aldrich (98–99%, 97%, and 99% purity, respectively). The molecular structures are shown in Figure 1.

For low Z elements the electron yield is higher than the fluorescence, which makes total electron yield (TEY) the preferred detection mode in the soft X-ray region. Additionally, for TEY the sample should be a rather good conductor in order to avoid spurious effects from self-charging, the surface should be homogeneous, and the experiment is by its nature windowless. TEY is then unsuitable for liquid samples. Though giving lower yield, fluorescence yield (FY) detection is more versatile with respect to the aggregation state of the sample and the rather low conductivity of many organic compounds has no effect, contrary to TEY. Care should be taken with particle sizes[30] to avoid self-absorption. Both collection modes (TEY and FY) were used in this paper.

Experimental data for DBTS have been collected in ANKA at the XAS beamline. Data for DLM were collected at the LUCIA beamline in SLS-Villigen while the spectrum of DBT was collected at ID 21 in ESRF-Grenoble. The XAS beamline at ANKA was equipped with a double Si(111) crystal monochromator and a system filled with 90 mbar N_2 gas that contained the sample and the ionization chamber as well (with a 12 μm Kapton entrance window). A Si multicathode detector (Vortex, 50 mm^2 area) was used for the FY detection. Powder samples were finely spread on sulfur-free Kapton tape. Calibration was performed with $ZnSO_4$ as reference for which the peak position of the white line was assigned a value of 2481.44 eV. The LUCIA beamline in SLS was equipped with a Kirkpatrick–Baez mirror (defocused), a Si(111) monochromator, a vacuum chamber for the sample mounting, and a Si drift diode detector inserted within. The Be window from the monochromator to the chamber was removed for data collection (in vacuum). The setup allows simultaneous collection of TEY and FY data; in the present case the data were collected in TEY mode. The sample was compressed in a pellet without any additive, and mounted on indium over a Cu plate. Calibration was performed with K_2SO_4 as standard, assigning a value of 2482.6 eV to the white line position. The X-ray microscopy beamline ID 21 in

ESRF[31] was equipped with a Si(111) monochromator. The focusing lens was removed to obtain an unfocused beam. Data were collected in fluorescence with a Ge detector. Calibration was achieved with use of K_2SO_4 as described above. Samples were in this case prepared by spreading a fine powder on sulfur-free tape and choosing four homogeneous spots on the sample by using the in situ microscope.

XANES data were collected in the range −100 to +400 eV with respect to the edge position. Data reduction was performed with the package ATHENA.[32−34] Background reduction was carried out by using the Autobackup routine.[35]

DFT simulations were performed by using the code StoBe-deMon.[27] The nonlocal exchange functional from Perdew and Wang[36] and the correlation functional from Perdew[37,38] were used. The transition potential or half-core-hole (HCH) approach[39] was used to generate the excitation, by removing half an electron from the 1s. The core-excited sulfur was described by using the IGLO III basis[40] to allow core relaxation. The basis sets used were the following: (621/41/1) for C, O, and N, and (311/1) for H. The auxiliary basis sets (N^C-s, N^C-spd; N^{XC}-s, N^{XC}-spd) used to fit the density in the Coulomb interaction and to interpolate the exchange-correlation potential over the numerical grid were (5, 4; 5, 4) for S, (5, 2; 5, 2) for C, N, and O, and (3, 1; 3, 1) for H. The code utilizes a double basis set approach adding a large number of functions during a second step of the calculation for more diffuse states (Rydberg and the near continuum). The dipole transition elements were calculated between the initial and final states, which in the transition potential approach are both described with the same set of molecular orbitals. Effects of the core-hole potential were investigated by applying both the transition potential half-core-hole (HCH) approach and the full-core-hole approximation (FCH), where one hole was created in the 1s, and the electron was removed from the calculation.

The spectra are energy calibrated by calculating the lowest core-excited state in the presence of a single hole in the 1s level.[41] The spectra were shifted by +7.4 eV to account for the relativistic correction.[28] An additional shift of 0.3 eV (DLM), 0.5 eV (DBT) was needed, in agreement with the results of Damian-Risberg et al.[29] For DBTS the calculated spectrum was shifted 1.5 eV. The calculated transitions should be broadened to obtain the spectra, ideally with a Voigt line profile. From the calculation there is, however, no information on the parameters necessary to build the profile and for these solid samples the line profile furthermore becomes complicated by excitation of phonons, band structure effects, screening, local disorder, etc.; the calculated resonances were instead broadened by simply using Gaussian functions with a broadening linearly dependent on the energy. Below the edge the broadening was fixed at 0.5 eV while the region between the threshold of the edge and +20 eV was increased linearly to a maximum value of 4 eV.

In the transition potential half-core-hole approach the response of the molecular ion core to the presence of the excited electron is neglected. To analyze the effect of full relaxation of the states above the absorption edge, the Kohn−Sham excited state (ΔKS) DFT method[41] was applied in specific calculations to variationally determine the core-excited states within +15 eV of the absorption edge; in the case of DBT the effect of relaxation on the transition intensities was explored by also computing the nonorthogonal transition moments between the variationally determined ground state and each core-excited state. The wave functions were in this case taken as the Kohn−Sham determinants with proper singlet-coupling of the core-excited state. The
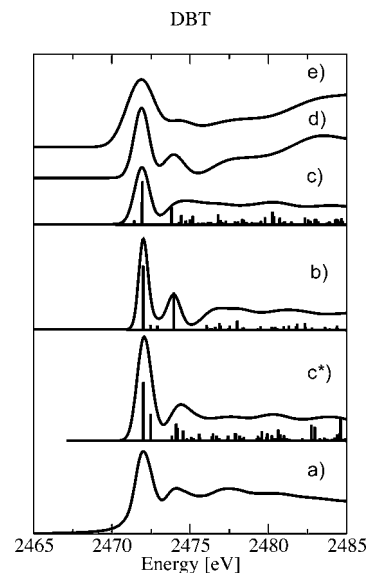
DBT

Figure 2. Experiment and simulations for dibenzothiophene. From bottom to top: (a) experiment, (c*) relaxed with nonorthogonal transition moments, (b) FCH, (c) HCH, (d) Löwdin HCH DOS, and (e) Löwdin ground state DOS. The transitions before broadening are shown as sticks.

five lowest transitions (in the original molecular basis) were obtained in this way while the remaining spectrum was generated based on the density of the last core-excited state and the full augmentation basis. Orthogonality was maintained by orthogonalizing the additional states against the variationally determined core-excited states.

The HCH and the ground state α spin densities of unoccupied states (DOS) were calculated for all compounds by using the Löwdin DOS, obtained for an orthonormal basis. The electronic densities for the first unoccupied states that contribute to the white line are referred to in general as "LUMOs" and were plotted with MOLEKEL.[42]

Results and Discussion

We start by comparing the experimental spectra with the transition potential half-core-hole calculations (HCH), which are expected to give the best simulations. Below we will compare the HCH spectra with the full-core-hole (FCH) and density of states methods. In the case of dibenzothiophene we also make a comparison with the nonorthogonal transition moment calculation based on the variationally relaxed core-excited states.

a. Dibenzothiophene (DBT). Figure 2 shows the comparison of the experimental DBTS spectrum (Figure 2a) with three XANES simulations respectively with relaxed states (Figure 2c*), FCH (Figure 2b), and HCH (Figure 2c) and with two DOS curves for the HCH case (Figure 2d) and for the ground state (Figure 2e). The HCH calculation (Figure 2c) reproduces well the main peak at 2472 eV and the resonance at about 2474 eV while the second resonance, which in the experiment appears around 2477 eV, is obtained at higher energy in the calculation.

The FCH calculation (Figure 2b) gives a good approximation to the experimental data and actually improves over the HCH simulation (Figure 2c) in terms of the second and third resonances. We note, however, that there is no theoretical justification to completely neglect the influence of the initial state in the evaluation of the oscillator strengths as is done when the same orbitals are used to represent both states in this case.
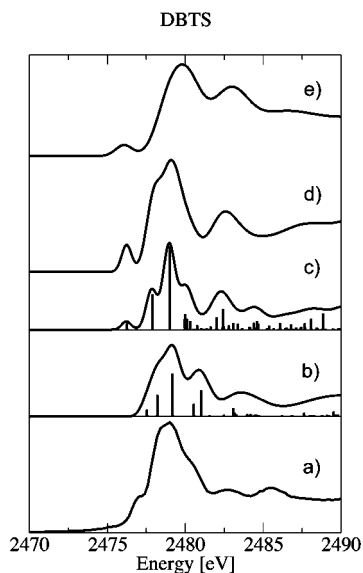
Interpretation of Sulfur K-Edge XANES Spectra

J. Phys. Chem. A, Vol. 113, No. 12, 2009 **2753**

DBTS

Figure 3. Experiment and simulations for dibenzothiophene sulfone. From bottom to top: (a) experiment, (b) FCH, (c) HCH, (d) Löwdin HCH, and (e) Löwdin ground state. The transitions before broadening are shown as sticks.

DLM

Figure 4. Experiment and simulations for DL-methionine. From bottom to top: (a) experiment, (b) FCH, (c1) HCH, linear broadening [0.5−2 eV], (c2) HCH linear broadening, [0.5−4 eV], (d) Löwdin HCH, and (e) Löwdin ground state. The transitions before broadening are shown as sticks.

The XANES of DBT has also been calculated by including the relaxation of the first excited states and taking the nonorthogonal transition moments (Figure 2c*). This improves the shape of the white line and the first resonance and reproduces rather accurately the positions of all three experimentally observed resonances in the continuum. In total, the relaxed DBT spectrum with nonorthogonal transition moments (Figure 2c*) simulates the XANES spectrum (Figure 2a) rather closely.

In the case of DBT, the Löwdin projected unoccupied DOS for the half-core-hole (Figure 2d) are in the low-energy part similar to the experimental spectrum (Figure 2a), where the agreement with the first two peaks is even better than that for the uncorrected HCH transition potential (Figure 2c) spectrum. The unoccupied DOS for the ground state (Figure 2e) shows similar features as the half-core-hole calculations, but with a broader edge peak and the second peak shifted to higher energy due to the omission of the core-hole potential.

We will analyze the spatial distribution of the first few lowest unoccupied molecular orbitals (LUMO) for the HCH calculation (Figure 2c), shown as sticks in the spectrum. The LUMO is the low intensity transition at 2471.45 eV, and with increasing energy follow the second (LUMO+1) and third (LUMO+2) unoccupied orbitals, at 2471.9 and 2471.95 eV, respectively. For DBT the LUMO contour plot (see Figure 5) shows no significant intensity at the sulfur, only a slight p_z character. The LUMO+1 shows an antibonding π^*_g S−C bond. In the LUMO+2 the S−C contribution is a combination of a C hybrid sp (s and mainly p_z) and sulfur p_y and p_x character.

b. Dibenzothiophene sulfone (DBTS). Figure 3 shows the comparison of the experimental DBTS spectrum (Figure 3a) with two XANES simulations, respectively FCH (Figure 3b) and HCH (Figure 3c), and with two DOS curves for the HCH case (Figure 3d) and for the ground state (Figure 3e). The HCH simulation (Figure 3c) reproduces the main features of the experimental spectrum, but the shoulder at about 2477 eV is found as a separate feature at 2476 eV in the calculation, and the two resonances of the white line at about 2477.8 and 2478.9 eV and the shoulder at the high energy side of the white line at 2480.5 eV are well reproduced in the theoretical spectrum, though too sharp. The simulation also reproduces the two
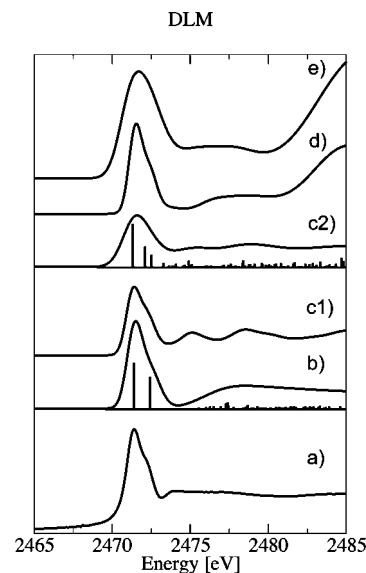
resonances above the edge, at about 2482 and 2485 eV. There is some disagreement with the experiment in the intensity, and the positions of the peaks are a little shifted to lower energy in the calculation.

In the case of DBTS, the agreement of the FCH (Figure 3b) calculated spectrum with experiment is not good. The leading shoulder has disappeared and is probably part of the main structure. The main edge structure is reproduced but the resonances at 2482 and 2485 eV are shifted to lower energy. It can be concluded that the FCH calculation pulls down the states too far toward the edge, in comparison with experiment.

In DBTS, the high number of transitions contributing to those two resonances above the edge does not allow performing stepwise relaxation of the low-lying core-excited states in a reliable manner, and it was not attempted except for the first transition used to calibrate the energy position of the spectra.

The Löwdin DOS spectrum (Figure 3d) is similar to the transition potential spectrum, but with an increased broadening. The ground state DOS of DBTS has its small leading edge peak further separated from the main peak. The effect of a half-core-hole is visible by comparing spectra e and d of Figure 3. The leading small peak remains at the same energy, but all other states are pulled down by the core-hole potential. This effect is even stronger for the FCH spectrum calculation (Figure 3b).

The molecular orbitals corresponding to the most intense transitions (the LUMO, LUMO+3, and LUMO+5) for the HCH calculation are shown in Figure 6. The corresponding transitions are shown as sticks in Figure 3c, together with the simulated spectrum. The LUMO (at 2476.4 eV) has p_x character and the LUMO+3 (at 2478 eV) and the LUMO+5 (at 2479.16 eV) have stronger p_x and p_y characters and also "s" (sp²). The LUMO+1 (at 2477 eV), LUMO+2 (at 2477.6 eV), and LUMO+4 (at 2478.73 eV) have no significant p character. The LUMO+1, LUMO+2, and LUMO+4 have contributions from the "d" orbitals. Three transitions at about 2480.1 eV compose the right shoulder of the white line.

c. DL-methionine (DLM). Figure 4 shows the comparison of the experimental DLM spectrum (Figure 4a) with three XANES simulations, respectively FCH (Figure 4b) and HCH
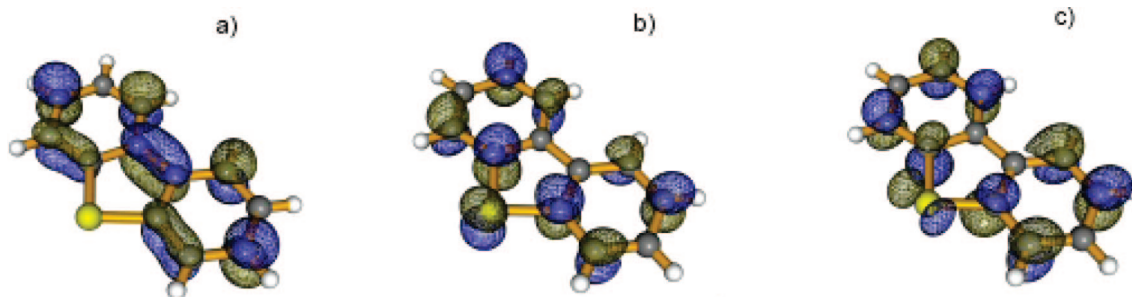
Figure 5. LUMOs composing the white line for DBT: (a) LUMO, (b) LUMO+1, and (c) LUMO+2.
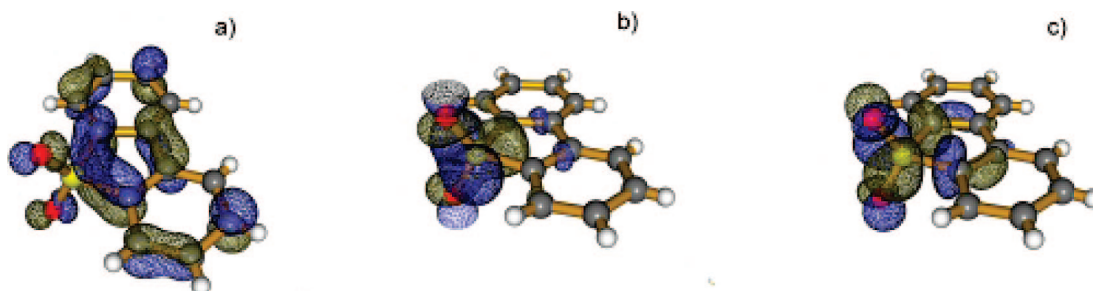

Figure 6. Strongest LUMOs composing the white line for DBTS: (a) LUMO, (b) LUMO+3, and (c) LUMO+5.
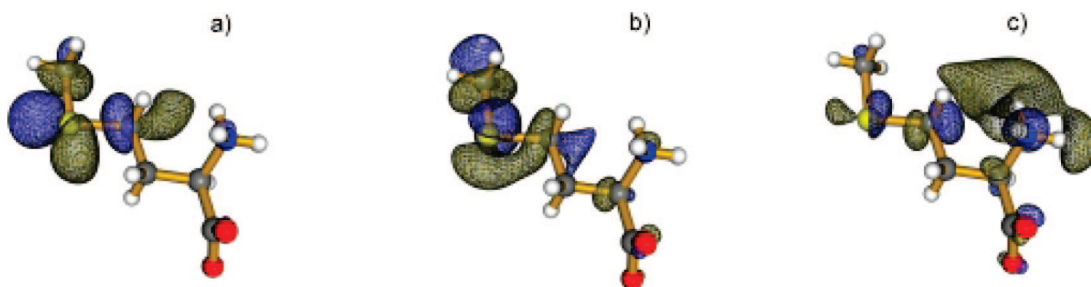

Figure 7. LUMOs composing the white line for DLM: (a) LUMO, (b) LUMO+1, and (c) LUMO+2.

(Figure 4, spectra c1 and c2), and with two DOS curves for the HCH case (Figure 4d) and for the ground state (Figure 4e). Figure 4 shows the comparison of the HCH simulation (Figure 4, spectra c1 and c2) with the experimental DL-methionine spectrum (Figure 4a). For this aliphatic sulfur compound, the HCH simulation provides all the features of the spectrum. This is similar to the findings of Damian-Risberg et al.[29] for L-methionine in solution. The white line consists of three contributions yielding together an asymmetric line shape. The calculation in Figure 4c1 uses a broadening linearly increasing up to 2 eV, which reproduced the asymmetric edge but which is too sharp at higher energies. Figure 4c2 uses a maximum broadening of 4 eV, which, however, is too broad at the edge.

The FCH spectrum (Figure 4b) simulates the main edge, but the intensity after the edge is poorly reproduced. For DLM, an upper limit of 8 eV for the broadening was necessary, in order to smear out sharp details. In DLM there is an important contribution already to the low-lying states from the augmentation basis in the transition potential calculation such that the variational relaxation of the core-excited states could not be performed in a reliable way. Similarly to DBTS, the Löwdin DOS spectrum is similar to the HCH transition potential spectrum, but with an increased broadening, before breaking down at about 8 eV above the edge.

The LUMOs at the edge for the HCH calculation are shown in Figure 7. The transitions corresponding to those LUMOs are shown as sticks together with the simulated spectrum in Figure

4c2, with the LUMO at 2471.3 eV, the LUMO+1 at 2472.12 eV, and the LUMO+2 at 2472.53 eV. In DLM the LUMO for sulfur shows some s character but more important are the p_x and p_y characters. In the LUMO+1 the "s" contribution is more important, being almost the only important contribution in the LUMO+2. The p_x and p_y character is more important in LUMO+1 than in the LUMO+2.

Discussion

The ionicity values determined from the DFT simulations underpin the systematic correlation between the effective nuclear charge and edge position.[13,43] In the HCH approximation, the ionicity values from the calculated Mulliken charges are in agreement with a shift of the edge toward higher energies for the lower effective charges: ionicities of 0.8, 0.11, and 0.08 for DBTS, DBT, and DLM, respectively, with the edge going from higher to lower energies in the same order.

The white lines for DBT and DLM look rather similar, but quite different from DBTS. Looking at the transitions, the white lines for DBT and DLM are composed of three resonances with different relative intensity ratio but with a rather similar overall shape for both compounds.

The calculated transitions give insights in the differences between the thiophenes and the amino acid. In DLM the sharp rise of the K-edge is explained by the very intense first transition. This is different from the thiophenes where the lowest energy

Interpretation of Sulfur K-Edge XANES Spectra

J. Phys. Chem. A, Vol. 113, No. 12, 2009 **2755**

(unbroadened) transition at about 2477 eV for DBTS or 2472 eV for DBT (see the sticks in Figures 3 and 2 for HCH) gives rise to a shoulder. Both DBT and DBTS show similar (unbroadened) transitions after the edge (see sticks in Figures 2 and 3 for HCH). The difference made by the sulfone is in the shoulders at the low- and high-energy sides of the white line. Though the sharp rise of the white line is similar for DBT and DLM, the calculated transitions uncover the different natures of the electronic structure of the two samples, which, due to the experimental and core-hole lifetime broadening, is not evident in the experiment. For thiophenic sulfur (DBT and DBTS) the calculated transitions show a similar pattern (an intense transition preceded by a less intense one). DLM shows a different electronic structure (with three transitions monotonically decreasing in intensity for increasing energy), as expected for a compound chemically very different (aliphatic sulfur). These results indicate the complications in assigning spectral features to structural characteristics, i.e., thiophene compounds vs. aliphatic compounds.

In the half-core-hole calculation, DBT is very similar to DLM. The oscillation at 2477 eV in DBT is reproduced only when including the relaxation of the first excited states due to the core-hole. The FCH approximation to the relaxation effects was applied to the three compounds. Only for DBT did we find agreement with the experiment for the oscillations after the edge. The white line intensities are higher than those in the HCH approximation. For DLM the enhancement of the white line seems in excess and the best agreement is found for a linear broadening of 0.5 to 8 eV in a range of 20 eV above the edge. In general, it is expected that the HCH describes the experiment better[39] in cases where the near-edge transitions mix valence and Rydberg character, while FCH enhances excitonic effects which may be significant in certain solid state systems with delocalized orbitals.[25] This expectation proved valid for DBTS and DLM, but not for DBT.

The spectra are derived from the matrix elements calculated with the DFT-transition state. The removal of the 1s electron lowers the energies for both the occupied and virtual molecular orbitals and the valence electronic structure is rearranged to screen the positive charge. The importance of considering the matrix transition elements and the core-hole can be pondered when comparing with the (core-hole) DOS and the GS DOS. The Löwdin DOS for HCH and the ground state show similar features, with some differences in the relative intensities. The HCH Löwdin DOS did not include the "diffuse" basis set, used for the XANES spectra computation, in order to avoid spurious contributions to the densities of other atoms, due to the long range of the diffuse basis functions. In spite of the high similarity of the HCH DOS with the experimental spectra, a better agreement is found for the DLM and DBTS by the actual calculation of the XANES, which can be due to the contributions from the diffuse basis to the XANES spectrum, which is not included in the DOS calculations, and to the contribution of the dipole transition element.

The similarity of the XANES among compounds with different functional groups and/or chemical nature still needs to be explained at the molecular level.

In DBT the strongest transitions are to orbitals with antibonding p_z character (Figure 5). The LUMO+2, with p_x, p_y character, shows the lowest intensity of the three transitions composing the white line.

For DBTS the strongest transitions are those to orbitals with p_x, p_y character (LUMO+3 and LUMO+5) (Figure 6). Interestingly, the first three transitions in the white line are mainly p_z, and p_x-p_y, respectively, similar to DBT. However, the intensities are different for the two compounds. Besides the contribution to the "p", the relatively significant contribution to the "d" orbitals in LUMO+1, LUMO+2, and LUMO+4 makes the orbitals very delocalized (Rydberg-like), which accounts for the low intensity of the respective transitions.

In DLM the strongest transitions are to orbitals with p_x, p_y character (LUMO and LUMO+1) (Figure 7) in contrast to the thiophenes where the ring structure favors the p_z character.

Final Considerations

The use of the diffuse augmentation basis sets in the half-core-hole calculations together with the inclusion of the relaxation of the first few excited states gives the best approximation to the experimental spectra, with a rather good agreement in the near-edge region. This region is dominated by transitions to bound states as well as strong scattering. The diffuse set allows describing highly delocalized Rydberg states as well as transitions to the continuum or scattering. The atom positions in the molecule generate, together with the electronic density, the potential for the excited electron; the excited state can then be obtained by solving for the time-independent wave function in this potential, as is done in the StoBe code, or, equivalently, by considering explicitly the scattering process as in real space full multiple scattering theory (FEFF).[44] For bound states the full, detailed potential and localized basis set used in StoBe constitute an advantage, while in the EXAFS region the multiple-scattering approach is superior; the localized basis gives a poor sampling of the continuum at higher energies. In a region above the edge both approaches should give equivalent results.

XANES (and XAS) belongs to the group of spectroscopies that happen in an excited state (together with Mössbauer), in contrast to ground state spectroscopies (like EPR). In the transition potential approach the core-hole and the relaxation of the transitions are included. In time-dependent DFT (TD-DFT), on the other hand, which is a more strict approach to excited states in DFT, the XANES is calculated from the ground state and the often very large response to the creation of the core-hole is estimated through the density−density response function. For optical spectroscopies in the valence region this approach is necessary, but for core excitations from a single, energetically well-separated core level the single-determinant description implicit in Kohn−Sham theory becomes a very good approximation; from an energetics viewpoint the huge relaxation effects from removing a core electron can be difficult to capture fully through the response based on the ground state density in TD-DFT, while they are explicitly included in the transition-potential approach. All these features of the local basis set and transition potential formalism enable a very accurate description of the XANES for a sufficiently large, but still limited, range above the edge.

The most distinctive feature in sulfur XANES is the huge range of variation in the edge position depending on the actual oxidation state of the sulfur. Experimentally it is known that the edges shift to higher energy with increased oxidation state of the absorber.[9,45] In our case, the ionicities are in agreement with the expected shift in the edge due to effective charge changes at the absorbing atom. DBTS shows the highest ionicity, as well as the shift of the edge toward higher energies as expected with the strongest transitions being of p_x, p_y character. Little electron density is found in the S−C or the S−O directions for the LUMO+3, while the LUMO+5 (the strongest line) shows more antibonding (sp) character in the S−C direction.

It has been shown that identical groups can lead to very different XANES.[43] We have shown here that similar XANES

2756 *J. Phys. Chem. A, Vol. 113, No. 12, 2009*

Mijovilovich et al.

may stem from different functional groups, posing a problem for speciation. The similar edge position and shape of the white line for DBT and DLM makes it difficult to differentiate between the two compounds. For biological speciation of sulfur this problem is not expected, while after the hydrogenation processes in crude oils, only thiophenes should be present. For samples where both species (aliphatic and thiophenes) are present, complementary studies should be done to determine the presence of aliphatics (in thiophenes). On the other hand, the good news for speciation is that the groups showing similar edge position still show differences in the shapes of their white lines (like significant broadening differences) and frequency of the higher oscillations where the differences stem from the different electronic structure of the groups.

References and Notes

(1) Rompel, A.; Cinco, R. M.; Latimer, M. J.; McDermott, A. E.; Guiles, R. D.; Quintanlha, A.; Krauss, R. M.; Sauer, K.; Yachandra, V. K.; Klein, M. P. *Proc. Natl. Acad. Sci. U.S.A.* **1998**, *95*, 6122.

(2) Pickering, I. J.; Prince, R. C.; Divers, T.; George, G. N. *FEBS Lett.* **1998**, *441*, 11.

(3) Yu, E. Y.; Pickering, I. J.; George, G. N.; Prince, R. C. *Biochim. Biophys. Acta* **2001**, *1527*, 156.

(4) Sandström, M.; Jalilehvand, F.; Damian, E.; Fors, Y.; Gelius, U.; Jones, M.; Salomé, M.; Gray, H. B. *Proc. Natl. Acad. Sci. U.S.A.* **2005**, *102*, 14165.

(5) Sandstrom, M.; Jalilehvand, F.; Persson, I.; Gelius, U.; Frank, P.; Hall-Roth, I. *Nature* **2002**, *415*, 893.

(6) Morra, M. J.; Fendorf, S. E.; Brown, P. D. *Geochim. Cosmochim. Acta* **1997**, *61*, 683.

(7) Majzlan, J.; Myneni, S. C. B. *Environ. Sci. Technol.* **2005**, *39*, 188.

(8) George, G. N.; Gorbaty, M. L. *J. Am. Chem. Soc.* **1989**, *111*, 3182.

(9) Waldo, G. S.; Mullins, O. C.; Penner-Hahn, J. E.; Cramer, S. P. *Fuel* **1992**, *71*, 53.

(10) Sarret, G.; Connan, J.; Kasrai, M.; Bancroft, G. M.; Charriè-Duhaut, A.; Lemoine, S.; Adam, P.; Albrecht, P.; Eybert-Bèrard, L. *Geochim. Cosmochim. Acta* **1999**, *63*, 3767.

(11) Knudsen, K. G.; Cooper, B. H.; Topsøe, H. *Appl. Catal. A* **1999**, *189*, 205.

(12) Wiltfong, R.; Mitra-Kirtley, S.; Mullins, O. C.; Andrews, B.; Fujisawa, G.; Larsen, J. W. *Energy Fuels* **2005**, *19*, 1971.

(13) Solomon, E. I.; Hedman, B.; Hodgson, K. O.; Dey, A.; Szilagyi, R. K. *Coord. Chem. Rev.* **2005**, *249*, 97.

(14) Sarangi, R.; DeBeer George, S.; Rudd, D. J.; Szilagyi, R. K.; Ribas, X.; Rovira, C.; Almeida, M.; Hodgson, K. O.; Hedman, B.; Solomon, E. I. *J. Am. Chem. Soc.* **2007**, *129*, 2316.

(15) De Groot, F. M. F.; Kotani, A. *Core level Spectroscopies of Solids*; Taylor & Francis: New York, 2008.

(16) Taillefumier, M.; Cabaret, D.; Flank, A.-M.; Mauri, F. *Phys. Rev. B* **2002**, *66*, 195107.

(17) Czyzyk, M. T.; De Groot, F. M. F. First-principle calculation of the x-ray Absorption spectra; 2nd european Conference on Progress in X-ray Synchrotron Radiation Research, 1990, Bologna.

(18) Weijs, P. J. W.; Czyzyk, M. T.; van Acker, J. F.; Speier, W.; Goedkoop, J. B.; van Leuken, H.; Hendrix, H. J. M.; de Groot, R. A.; van der Laan, G.; Buschow, K. H. J.; Wiech, G.; Fuggle, J. C. *Phys. Rev. B* **1990**, *41*, 11899.

(19) Czyzyk, M. T.; Potze, R.; Sawatzky, G. A. *Phys. Rev. B* **1992**, *46*, 3729.

(20) de Groot, F. M. F. *J. Electron Spectrosc. Relat. Phenom.* **1994**, *67*, 529.

(21) Grioni, M.; van Acker, J. F.; Czyzyk, M. T.; Fuggle, J. C. *Phys. Rev. B* **1992**, *45*, 3309.

(22) Soriano, L.; Abbate, M.; Fernandez, A.; Gonzalez-Elipe, A. R.; Sanz, J. M. *Surf. Interface Anal.* **1997**, *25*, 804.

(23) Degroot, F. M. F.; Faber, J.; Michiels, J. J. M.; Czyzyk, M. T.; Abbate, M.; Fuggle, J. C. *Phys. Rev. B* **1993**, *48*, 2074.

(24) Hetenyi, B.; De Angelis, F.; Giannozzi, P.; Car, R. *J. Chem. Phys.* **2004**, *120*, 8632.

(25) Cavalleri, M.; Odelius, M.; Nordlund, D.; Nilsson, A.; Pettersson, L. G. M. *Phys. Chem. Chem. Phys.* **2005**, *7*, 2854.

(26) Odelius, M.; Cavalleri, M.; Nilsson, A.; Pettersson, L. G. M. *Phys. Rev. B* **2006**, *73*, 1.

(27) Hermann, K.; Pettersson, L. G. M.; Casida, M. E.; Daul, C.; Goursot, A.; Koester, A.; Proynov, E.; St-Amant, A.; Salahub, D. R.; Carravetta, V.; Duarte, H.; Godbout, N.; Guan, J.; Jamorski, C.; Leboeuf, M.; Malkin, V.; Malkina, O.; Nyberg, M.; Pedocchi, L.; Sim, F.; Triguero, L.; Vela, A. StoBe-deMon code, 2001.

(28) Damian-Risberg, E.; Eriksson, L.; Mink, J.; Pettersson, L. G. M.; Skripkin, M. Y.; Sandström, M. *Inorg. Chem.* **2007**, *46*, 8332.

(29) Damian-Risberg, E.; Jalilehvand, F.; Leung, B.; Pettersson, L. G. M.; Sandström, M. Submitted for publication, 2008.

(30) Pickering, I. J.; George, G. N.; Yu, E. Y.; Brune, D. C.; Tuschak, C.; Overmann, J.; Beatty, J. T.; Prince, R. C. *Biochemistry* **2001**, *40*, 8138.

(31) Susini, J.; Salome, M.; Fayard, B.; Ortega, R.; Kaulich, B. *Surf. Rev. Lett.* **2002**, *9*, 203.

(32) Ravel, B.; Newville, M. *J. Synchrotron Radiat.* **2005**, *12*, 537.

(33) Ravel, B. http://cars9.uchicago.edu/~ravel/software/exafs/, 2005.

(34) Newville, M. *J. Synchrotron Radiat.* **2001**, *8*, 322.

(35) Newville, M.; Livins, P.; Yacoby, Y.; Rehr, J. J.; Stern, E. A. *Phys. Rev. B* **1993**, *47*, 14126.

(36) Perdew, J. P.; Yue, W. *Phys. Rev. B* **1986**, *33*, 8800.

(37) Perdew, J. P. *Phys. Rev. B* **1986**, *33*, 8822.

(38) Perdew, J. P. *Phys. Rev. B* **1986**, *34*, 7406.

(39) Triguero, L.; Pettersson, L. G. M.; Ågren, H. *J. Phys. Chem. A* **1998**, *102*, 10599.

(40) Kutzelnigg, W.; Fleischer, U.; Schindler, M. *NMR-basic principles and progress*; Springer: New York, 1990.

(41) Kolczewski, C.; Puttner, R.; Plashkevych, O.; Ågren, H.; Staemmler, V.; Martins, M.; Snell, G.; Schlachter, A. S.; Sant'Anna, M.; Kaindl, G.; Pettersson, L. G. M. *J. Chem. Phys.* **2001**, *115*, 6426.

(42) *MOLEKEL*. http://bioinformatics.org/molekel.

(43) Sarangi, R.; Frank, P.; Hodgson, K. O.; Hedman, B. *Inorg. Chim. Acta* **2008**, *361*, 956.

(44) Ankudinov, A. L.; Ravel, B.; Rehr, J. J.; Conradson, S. D. *Phys. Rev. B* **1998**, *58*, 7565.

(45) Hedman, B.; Frank, P.; Penner-Hahn, J. E.; Roe, A. L.; Hodgson, K. O.; Carlson, R. M. K.; Brown, G.; Cerino, J.; Hettel, R.; Troxel, T.; Winick, H.; Yang, J. *Nucl. Instrum. Methods Phys. Res., Sect. A* **1986**, *246*, 797.

JP806823C